This is a peer-reviewed, author's accepted manuscript of the following conference output: Vlachakis, C., Perry, M., & McAlorum, J. (2021). 3D printed self-sensing alkali-activated coatings for civil infrastructure. In *2021 IEEE International Instrumentation and Measurement Technology Conference (I2MTC)* (pp. 1-5). (IEEE International Instrumentation and Measurement Technology Conference). IEEE. https://doi.org/10.1109/i2mtc50364.2021.9459899

3D printed self-sensing alkali-activated coatings for civil infrastructure

Christos Vlachakis
Dept. of Civil & Environmental Engineering
University of Strathclyde
Glasgow, UK
christos.vlachakis@strath.ac.uk

Marcus Perry
Dept. of Civil & Environmental Engineering
University of Strathclyde
Glasgow, UK
m.perry@strath.ac.uk

Jack McAlorum
Dept. of Civil & Environmental Engineering
University of Strathclyde
Glasgow, UK
jack.mcalorum.strath.ac.uk

***Abstract*— Monitoring civil infrastructure is paramount due to the ageing of existing civil infrastructure. Apart from electronic devices, self-sensing materials are also used for these types of applications. In this paper, we present 3D printed self-sensing coatings for civil infrastructure. The coating is an alkali-activated material, which attains similar properties to ordinary Portland cement binders but is more electrically conductive due to the alkali ions in the matrix. The coatings were printed onto concrete cubes and glass fiber reinforced plastic sheets to investigate their strain response under cyclic loading in compression and tension. The electrical response under compression presented reasonable repeatability among loading cycles. In tension, the patches presented repeatability issues in the first loading stage which eventually stabilized in later cycles. For both compression and tension the patches present a linear electrical response in regards to the applied strain. The gauge factor of the coatings was calculated as 1433 for compression and 383 for tension. 3D printed coatings have shown the potential of acting as a nondestructive evaluation method of existing infrastructure.**

Keywords—self-sensing material, alkali-activated materials, additive manufacturing, strain sensor, coating

I. Introduction

Monitoring the structural health of civil infrastructure has been a main focus in sensing applications. This has led to the use and incorporation of external sensing devices such as strain gauges and fiber optic sensors for strain and temperature detection. Apart from electronic devices, self-sensing materials have also been used in sensing applications. In this case these materials simultaneously act as a structural component and as a sensing mechanism. Favorable candidates for self-sensing materials are alkali-activated materials (AAM). These materials attain similar mechanical properties to ordinary Portland cement (OPC) binders [1]. However they are inherently more electrically conductive owing to their unique means of fabrication. AAM are formulated by mixing an aluminosilicate precursor, typically metakaolin (calcined clay), fly ash and ground granulated blast furnace slag, and an alkaline solution, typically a mixture of an alkali silicate and alkali hydroxide, usually sodium (Na^+) or potassium (K^+) [2]. The alkali ions in the AAM matrix make the material more conductive due to enhanced ionic conductivity [3]. As a result, AAM have been successful used as strain [4], temperature [5] and moisture sensors [6] . While it is common practice to incorporate conductive filler such as carbon fiber, carbon nanotubes, carbon black etc. AAM have seen numerous sensing applications without the use of conductive filler [5]–[7].

AAM have also been use for coating and repair applications [8]–[11]. AAM are able to chemically bond onto concrete substrates. The positive calcium ions (Ca^{2+}) from the OPC concrete surface charge balance the negatively charged aluminium ions (Al^{3+}) in AAM binders creating a chemical bond at the interface of these two materials [12].

Cementitious materials have seen a new means of fabrication over the past decade in the form of additive manufacturing. Cement-based materials are able to be extruded through a nozzle in a layer-by-layer process without the use of additional framework [13]–[15]. This has allowed for more complex designs and numerous applications. Apart from the fabrication of structural elements [13], [16] additive manufacturing has also been used in deploying coatings onto existing infrastructure [5], [7], for insulative applications [17], electronic packaging [18] and architectural purposes [19].

In this paper we expand on the current research of 3D printed self-sensing AAM coatings. The purpose of this study is to investigate the feasibility of monitoring existing structures with a cementitious material that, apart from a protective coating, can also act as a strain sensor. The means of fabrication of the printed self-sensing coating is presented and the strain sensing capabilities under compression and tension for this material are investigated.

II. Materials and Methodology

A. Materials

Metakaolin was selected as the precursor for this study as it has showcased high strength and consistent performance in previous applications as a standalone element [20] and as a repair for concrete substrates [8] . Metakaolin was produced by calcining highly refined kaolin originating from south England, in an electric furnace at 800 °C for 2 hours. The precursor was left to cool down inside the furnace and was

This work was supported in part by the Royal Society (grant number RG160748), and the Oil & Gas Innovation Centre (OGIC).

then stored in sealed containers until use. Commercially supplied densified silica fume was also added to the mix for greater densification [15]. The properties of kaolin and silica fume are presented in Table 1. Polyvinyl alcohol PVA fibers (3 mm) were also added to the mix to improve adhesion with the concrete substrate, crack resistance [8] and shape stability [21]. The alkaline activator was prepared by mixing commercial sodium silicate (Na_2O = 8.5%, SiO_2 = 27.8%, H_2O = 63.7%) and sodium hydroxide 10 M. The mass ratio of solution used for this experiment was Na_2SiO_3:NaOH =2.0. The solution was left to cool down for at least 24h prior to use.

The mix was required to achieve adequate adhesion with the concrete substrate while being able to maintain dimensional integrity. This essentially requires a series of trial and error. Following the investigation outlined in [5], the solid to liquid ratio of the paste was set at 0.90 to balance these requirements. The precursor consisted of 95% metakaolin and 5% silica fume by mass. A total weight of 0.5% of PVA (3 mm) fibers was added to the mix. Metakaolin, silica fume and PVA fibers were first dry mixed for 5 minutes to ensure homogeneity among the dry constituents. Following that, the activator was then poured into the dry materials and mixed for at least 10 minutes until a homogeneous slurry was obtained.

TABLE 1: MATERIAL PROPERTIES

	SiO_2	**Al_2O_3**	**Mean particle size**
Kaolin	47% mass	38% mass	10 µm
Silica fume	92.5%	-	≤1 µm

B. 3D printing

For extrusion, a progressive cavity dosing pen was installed onto the x-y gantry axis of a commercial 3D printer. The filament paste for extrusion was inserted into the cartridge in which air pressure of 2 bar was applied to force the material to flow into the screw extruder's dispensing cavity. The printing setup is depicted in Fig. 1.

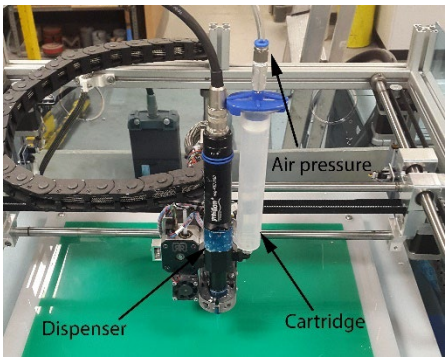

Fig. 1. 3D printing setup with dispensing unit mounted on axis and air pressurized feed cartridge.

The nozzle size of the extruder was 18 G (0.84 mm) and the layer height was 0.66 mm for greater compaction between layers. The print speed was set at 40 mm/s.

For compressive strain sensing a double layered patch with dimensions 90 mm x 90 mm was printed onto a 100 mm concrete cube. The concrete surface was wire brushed to remove the top weak cement layer and expose the aggregates to ensure greater adhesion with the deposited coating [22]. For tensile testing, a double layered patch with dimensions 30 mm x 50 mm was printed onto a glass fiber reinforced plastic (GFRP) tensile testing piece. GFRP was selected instead of steel to avoid any potential electrical interferences from the substrate. A drawing of the GFRP is illustrated in Fig. 2 and the dimensions of the tensile piece are presented in Table 2. Sand was glued onto the surface of the GFRP to allow proper interlocking between the materials in order to achieve adequate adhesion between the substrate and the sensing patch.

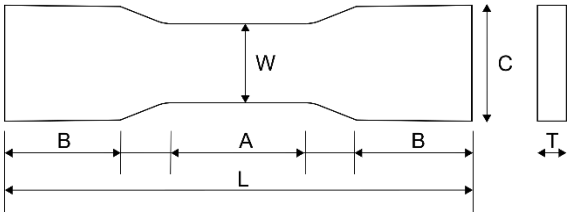

Fig. 2. Schematic drawing of GFRP tensile testing piece

TABLE 2: DIMENSIONS OF GFRP

Dimension name	**Dimensions (mm)**
A	60
B	50
C	50
L	200
T	3
W	35

Stainless steel electrodes were placed at the corners of the patches following the van der Pauw configuration [23]. The samples were then sealed in a plastic container and cured in environmental chamber under ambient conditions for 28 days until testing. Fig. 3 shows an image of a printed patch for compressive and tensile testing respectively.

Fig. 3. Metakaolin based printed patch concrete substrate (left) GFRP substrate (right).

C. Electrial testing

The samples were interrogated with an electrical impedance analyser using a four-probe set up. For compressive testing the specimen was placed onto a universal loading cell with a maximum load capacity of 500 kN. The cube was loaded incrementally up to 50 kN and then unloaded with a step of 10 kN. For tensile testing, the tensile piece was loaded up to 200 N and then unloaded with a loading step of 40 N. In both cases the voltage applied was set at V = 10 mV at an alternate current (AC) frequency between 1 kHz-10 kHz. The current, I, was measured, allowing electrical impedance to be calculated via V = IZ. The applied loads in both cases were kept low to avoid any damage to the patches to allow for repeatable and reversible sensing [24]. In order to ensure a constant testing environment, the samples were wrapped with plastic film to maintain a constant humidity. The effect of the

plastic film on loading was deemed insignificant. The temperature of the surrounding environment was also measured with an external temperature sensing device. The temperature of the testing vicinity remained constant and was therefore accepted to not influence the strain sensing investigation. Three measurements were acquired for each load and each sample was tested for a total of three load cycles. For data analysis, a frequency of 5 kHz was chosen.

III. Results and Discussion

Fig. 4 & 5 depicts the fractional change in impedance against time for compressive and tensile strain respectively. The fractional change in impedance was calculated via (1).

$$\Delta Z/Z_0 \quad (1)$$

where Z_0 = initial impedance under no applied load, $\Delta Z=Z_i-Z_0$ the change in impedance in respect to the initial impedance. Under compression it can be seen that the impedance decreases under applied load and increases when the load is removed.

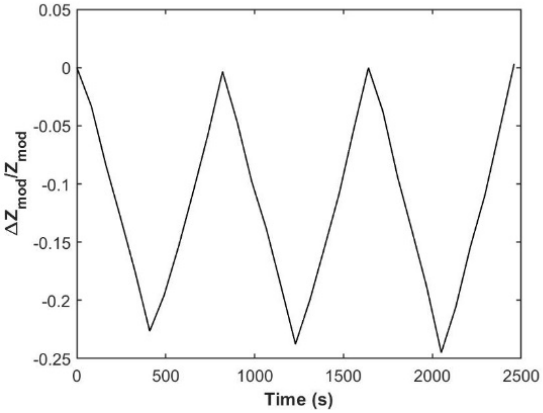

Fig. 4. Fractional change in impedance against time of AAM printed patch under compressive load.

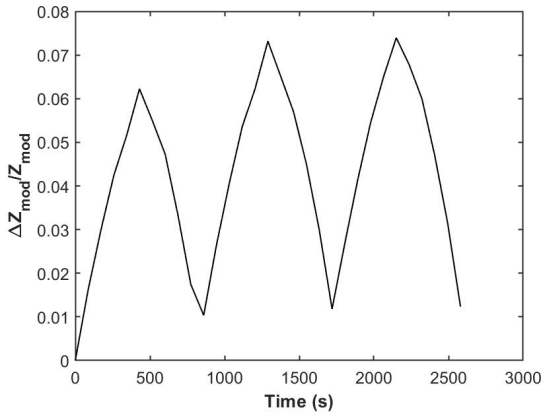

Fig. 5. Fractional change in impedance against time of AAM printed patch under tensile load

Under tension, the impedance increases as load is applied and decreases once the load is removed. This is in line with the expected behavior of self-sensing cementitious materials [25]–[29]. The sensing response of the patch in compression showcases a fairly repeatable behavior. Under tension, however, the patch displays slight repeatability issues primarily during the first loading cycle which eventually level out. This behavior could be attributed to the patch conforming to the substrate and due to minor damage in the matrix which resulted into a permanent impedance change throughout the subsequent sensing cycles. It can be inferred that the repeatability issues can also be a result of the inherent weaker tensile behavior of cementitious materials as a whole.

The sensing patches in this application are free of conductive filler. The changes in the electrical properties in AAM under these circumstances have been attributed to ion migration of the alkali metal ions (Na^+ and K^+) in the matrix [25], [30]. In the current application, the change in impedance is due to the migration of the Na^+ ions. It has been speculated that compression promotes ion migration as the distance between the available vacant sites that accommodate the alkali ions shortens thus leading to decreased impedance. In a similar manner, tension has been mentioned to hinder ion migration as the distance between these sites increases therefore impedance increases [25], [30]. While this mechanism has been generally accepted for these types of applications, it still warrants further investigation.

The performance of strain sensors is generally evaluated by the gauge factor (GF). The gauge factor indicates the fractional change of electrical properties in regards to the respective strain. The gauge factor is calculated by (2):

$$k= (\Delta Z/Z_0)/\varepsilon \quad (2)$$

where k = gauge factor, Z_0 = initial impedance under no applied load, $\Delta Z =Z_i-Z_0$ the change in impedance in respect to the initial impedance and ε= applied strain. The applied strain can be calculated through (3):

$$\varepsilon=\sigma/E \quad (3)$$

where σ = stress and E = modulus of elasticity. In this application the modulus of elasticity for concrete was 30 GPa and 5 GPa for the GFRP. Fig. 6 & 7 depict the fractional increase in impedance versus the applied strain for upward loading of the second loading cycle for compression and tension respectively.

The sensing patches present a linear behavior under compression and tension in this loading segment. Linear or a linear-like behavior is achievable by maintaining a low magnitude of applied loads [31]. This ensures the material will behave elastically and can avoid permanent deformation in the material which will in turn carry over to the electrical response of the matrix as well [32].

The gauge factor for compression and tension was calculated as 1433 and 383 respectively. The sensing under compression is relatively high in comparison to other self-sensing applications [33]–[35], however this sensing capacity is not uncommon for metakaolin AAM [28]. Furthermore it can be observed that the sensing capacity is higher for compression than it is in tension. Similar to the repeatability issues, this behavior could be attributed to the inherent higher compressive capabilities of AAM compared to the tensile behavior. Further investigation is required though to make a definitive claim.

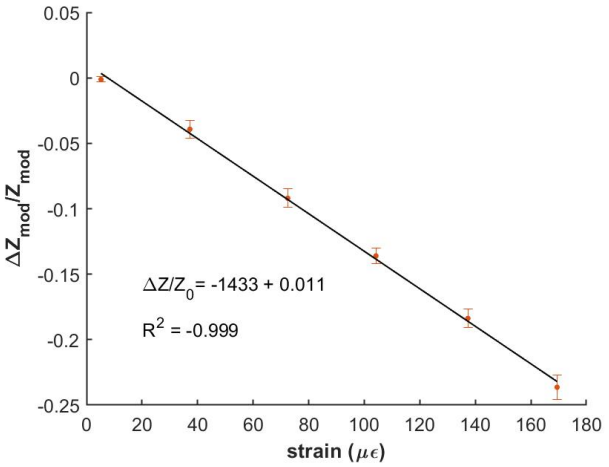

Fig. 6. Fractional increase in impedance against strain for AAM under compressive strain.

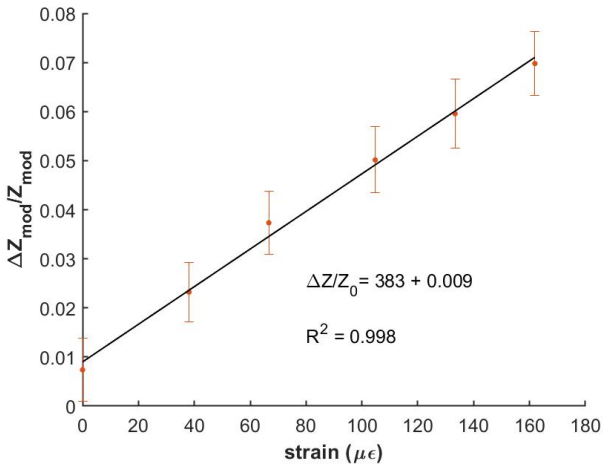

Fig. 7. Fractional increase in impedance against strain for AAM under tensile strain.

IV. Conclusions

In this work the sensing behavior of extruded patches under compression and tension was investigated. AAM patches were 3D printed onto concrete and GFRP substrates. The patches in this application are free of conductive filler. The change in impedance is speculated to occur due to the changes in the ion hopping distances the alkali metal ions must overcome, as a result the impedance decreases in compression and increases in tension. The sensing capability in both tension and compression presented reversible behaviour and reasonable repeatability among loading cycles. The sensing patches displayed a linear change in electrical properties in regards to the applied strain. The gauge factor under compression was calculated as 1433 and as 383 in tension. This enables 3D printed coatings to act as a non-destructive monitoring method for existing civil infrastructure.

References

[1] J. L. Provis and S. A. Bernal, "Geopolymers and Related Alkali-Activated Materials," *Annu. Rev. Mater. Res.*, vol. 44, no. 1, pp. 299–327, 2014, doi: 10.1146/annurev-matsci-070813-113515.

[2] J. L. Provis, "Alkali-activated materials," *Cem. Concr. Res.*, vol. 114, pp. 40–48, 2018, doi: 10.1016/j.cemconres.2017.02.009.

[3] X. M. Cui, G. J. Zheng, Y. C. Han, F. Su, and J. Zhou, "A study on electrical conductivity of chemosynthetic Al2O3-2SiO2geoplymer materials," *J. Power Sources*, vol. 184, no. 2, pp. 652–656, 2008, doi: 10.1016/j.jpowsour.2008.03.021.

[4] M. Perry, M. Saafi, G. Fusiek, and P. Niewczas, "Hybrid optical-fibre/geopolymer sensors for structural health monitoring of concrete structures," *Smart Mater. Struct.*, vol. 24, no. 4, 2015, doi: 10.1088/0964-1726/24/4/045011.

[5] C. Vlachakis, M. Perry, L. Biondi, and J. Mcalorum, "3D printed temperature-sensing repairs for concrete structures," *Addit. Manuf.*, vol. 34, no. August, p. 101238, 2020, doi: 10.1016/j.addma.2020.101238.

[6] L. Biondi, M. Perry, J. McAlorum, C. Vlachakis, and A. Hamilton, "Geopolymer-based moisture sensors for reinforced concrete health monitoring," *Sensors Actuators, B Chem.*, vol. 309, no. 15, p. 127775, 2020, doi: 10.1016/j.snb.2020.127775.

[7] J. McAlorum, M. Perry, C. Vlachakis, L. Biondi, and B. Lavoie, "Robotic spray coating of self-sensing metakaolin geopolymer for concrete monitoring," *Autom. Constr.*, vol. 121, no. October 2020, p. 103415, 2021, doi: 10.1016/j.autcon.2020.103415.

[8] C. Zanotti, P. H. R. Borges, A. Bhutta, and N. Banthia, "Bond strength between concrete substrate and metakaolin geopolymer repair mortar: Effect of curing regime and PVA fiber reinforcement," *Cem. Concr. Compos.*, vol. 80, pp. 307–316, 2017, doi: 10.1016/j.cemconcomp.2016.12.014.

[9] R. Robayo-Salazar, C. Jesús, R. Mejía de Gutiérrez, and F. Pacheco-Torgal, "Alkali-activated binary mortar based on natural volcanic pozzolan for repair applications," *J. Build. Eng.*, vol. 25, no. April, p. 100785, 2019, doi: 10.1016/j.jobe.2019.100785.

[10] V. A. Nunes, P. H. R. Borges, and C. Zanotti, "Mechanical compatibility and adhesion between alkali-activated repair mortars and Portland cement concrete substrate," *Constr. Build. Mater.*, vol. 215, pp. 569–581, 2019, doi: 10.1016/j.conbuildmat.2019.04.189.

[11] Z. Zhang, X. Yao, and H. Wang, "Potential application of geopolymers as protection coatings for marine concrete III. Field experiment," *Appl. Clay Sci.*, vol. 67–68, pp. 57–60, 2012, doi: 10.1016/j.clay.2012.05.008.

[12] F. Pacheco-Torgal, J. P. Castro-Gomes, and S. Jalali, "Adhesion characterization of tungsten mine waste geopolymeric binder. Influence of OPC concrete substrate surface treatment," *Constr. Build. Mater.*, vol. 22, no. 3, pp. 154–161, 2008, doi: 10.1016/j.conbuildmat.2006.10.005.

[13] T. A. M. Salet, Z. Y. Ahmed, F. P. Bos, and H. L. M. Laagland, "Design of a 3D printed concrete bridge by testing," *Virtual Phys. Prototyp.*, vol. 2759, no. May, pp. 1–15, 2018, doi: 10.1080/17452759.2018.1476064.

[14] S. C. Paul, Y. W. D. Tay, B. Panda, and M. J. Tan, "Fresh and hardened properties of 3D printable cementitious materials for building and construction," *Arch. Civ. Mech. Eng.*, vol. 18, no. 1, pp. 311–319, 2018, doi: 10.1016/j.acme.2017.02.008.

[15] B. Panda and M. J. Tan, "Experimental study on mix proportion and fresh properties of fly ash based geopolymer for 3D concrete printing," *Ceram. Int.*, vol. 44, no. 9, pp. 10258–10265, 2018, doi: 10.1016/j.ceramint.2018.03.031.

[16] B. Panda, S. C. Paul, N. A. N. Mohamed, Y. W. D. Tay, and M. J. Tan, "Measurement of tensile bond strength of 3D printed geopolymer mortar," *Meas. J. Int. Meas. Confed.*, vol. 113, no. April 2017, pp. 108–116, 2018, doi: 10.1016/j.measurement.2017.08.051.

[17] H. Alghamdi and N. Neithalath, "Synthesis and characterization of 3D-printable geopolymeric foams for thermally efficient building envelope materials," *Cem. Concr. Compos.*, vol. 104, no. July, 2019.

[18] Q. Sun, Y. Peng, H. Cheng, Y. Mou, Z. Yang, and D. Liang, "Direct ink writing of 3D cavities for direct plated copper ceramic substrates with kaolin suspensions," *Ceram. Int.*, vol. 45, no. 9, pp. 12535–12543, 2019, doi: 10.1016/j.ceramint.2019.03.191.

[19] S. S. L. Chan, R. M. Pennings, L. Edwards, and G. V. Franks, "3D printing of clay for decorative architectural applications: Effect of solids volume fraction on rheology and printability," *Addit. Manuf.*, vol. 35, no. May, p. 101335, 2020, doi: 10.1016/j.addma.2020.101335.

[20] R. Pouhet and M. Cyr, "Formulation and performance of flash metakaolin geopolymer concretes," *Constr. Build. Mater.*, vol. 120, pp. 150–160, 2016, doi: 10.1016/j.conbuildmat.2016.05.061.

[21] S. Chaves Figueiredo *et al.*, "An approach to develop printable strain hardening cementitious composites," *Mater. Des.*, vol. 169, 2019, doi:

10.1016/j.matdes.2019.107651.

[22] E. N. B. S. Júlio, F. A. B. Branco, and V. D. Silva, "Concrete-to-concrete bond strength. Influence of the roughness of the substrate surface," *Constr. Build. Mater.*, vol. 18, no. 9, pp. 675–681, 2004, doi: 10.1016/j.conbuildmat.2004.04.023.

[23] L. J. van der Pauw, "A method of measuring specific resistivity and and Hall effect of discs of arbitrary shape," *Philips Res. Reports*, vol. 13, no. 1, pp. 1–9, 1958.

[24] C. Vlachakis, M. Perry, and L. Biondi, "Self-Sensing Alkali-Activated Materials : A Review," *Minerals*, vol. 10, no. 10, pp. 1–34, 2020, doi: 10.3390/min10100885.

[25] M. Saafi, A. Gullane, B. Huang, H. Sadeghi, J. Ye, and F. Sadeghi, "Inherently multifunctional geopolymeric cementitious composite as electrical energy storage and self-sensing structural material," *Compos. Struct.*, vol. 201, no. July, pp. 766–778, 2018, doi: 10.1016/j.compstruct.2018.06.101.

[26] D.-Y. Yoo, S. Kim, and S. H. Lee, "Self-sensing capability of ultra-high-performance concrete containing steel fibers and carbon nanotubes under tension," *Sensors Actuators A Phys.*, vol. 276, pp. 125–136, 2018, doi: 10.1016/j.sna.2018.04.009.

[27] P. Rovnaník, I. Kusák, P. Bayer, P. Schmid, and L. Fiala, "Electrical and self-sensing properties of alkali-activated slag composite with graphite filler," *Materials (Basel).*, vol. 12, no. 10, pp. 1–16, 2019, doi: 10.3390/ma12101616.

[28] C. Lamuta, L. Bruno, S. Candamano, and L. Pagnotta, "Piezoresistive characterization of graphene/metakaolin based geopolymeric mortar composites," *MRS Adv.*, vol. 2, no. 61, pp. 3773–3779, 2017, doi: 10.1557/adv.2017.595.

[29] B. Han *et al.*, "Self-sensing cementitious composites incorporated with botryoid hybrid nano-carbon materials for smart infrastructures," *J. Intell. Mater. Syst. Struct.*, vol. 28, no. 6, pp. 699–727, 2017, doi: 10.1177/1045389X16657416.

[30] C. Lamuta, S. Candamano, F. Crea, and L. Pagnotta, "Direct piezoelectric effect in geopolymeric mortars," *Mater. Des.*, vol. 107, pp. 57–64, 2016, doi: 10.1016/j.matdes.2016.05.108.

[31] S. Ding, Y. Ruan, X. Yu, B. Han, and Y. Q. Ni, "Self-monitoring of smart concrete column incorporating CNT/NCB composite fillers modified cementitious sensors," *Constr. Build. Mater.*, vol. 201, pp. 127–137, 2019, doi: 10.1016/j.conbuildmat.2018.12.203.

[32] W. Wang, H. Dai, and S. Wu, "Mechanical behavior and electrical property of CFRC-strengthened RC beams under fatigue and monotonic loading," vol. 479, pp. 191–196, 2008, doi: 10.1016/j.msea.2007.06.046.

[33] J. L. Vilaplana, F. J. Baeza, O. Galao, E. Zornoza, and P. Garcés, "Self-sensing properties of alkali activated blast furnace slag (BFS) composites reinforced with carbon fibers," *Materials (Basel).*, vol. 6, no. 10, pp. 4776–4786, 2013, doi: 10.3390/ma6104776.

[34] M. Saafi *et al.*, "Graphene/fly ash geopolymeric composites as self-sensing structural materials," *Smart Mater. Struct.*, vol. 23, no. 6, 2014, doi: 10.1088/0964-1726/23/6/065006.

[35] S. Bi, M. Liu, J. Shen, X. M. Hu, and L. Zhang, "Ultrahigh Self-Sensing Performance of Geopolymer Nanocomposites via Unique Interface Engineering," *ACS Appl. Mater. Interfaces*, vol. 9, no. 14, pp. 12851–12858, 2017, doi: 10.1021/acsami.7b00419.